

# CFD simulation of a single-element wing in ground effect

Mattia Aurelio Martini, Sciper: 359665, e-mail: mattia.martini@epfl.ch

Francesco Sala, Sciper: 354790, e-mail: francesco.sala@epfl.ch

Nicolò Viscusi, Sciper: 358589, e-mail: nicolo.viscusi@epfl.ch

*EPFL, Switzerland*

**Abstract**—CFD simulations are widely used in aerodynamics applications, such as the automotive industry, to investigate the influence of aerodynamic appendages on the overall performance of the car itself. In the present work, a 2D CFD study of a single element wing operating in ground effect was conducted, in order to attain a reliable CFD model of such configuration: its reliability was assessed through a comparison with empirical data collected by Zerihan and Zhang in [1]. The same range of heights from the ground was investigated, and values of downforce coefficient  $c_L$ , drag coefficient  $c_D$  and pressure coefficient  $c_p$  were compared. The results attained show that downforce and drag coefficients are predicted with a relative error around 13% and 20%, respectively. Such results were considered proof of the reliability of the implemented simulation.

## I. INTRODUCTION

In the automotive industry, especially in the racing field, aerodynamic features are used to generate downforce which increases the grip of the vehicle and controls the flow over the entire frame. Zhang & Zerihan ([1]) investigated experimentally the aerodynamics of a single element wing in ground effect, varying the height of the wing from the ground  $h$ , in order to better understand the reason why the stall takes place when the wing is very close to the ground. In their work, carried out in a wind tunnel using a moving belt to mock real conditions, they were the first to explain that the stall is due to a large region of separated flow at the trailing edge. Additionally, they provided values of downforce coefficient  $c_L$ , drag coefficient  $c_D$  and pressure coefficients  $c_p$  for the above conditions, among other results. All these quantities were compared with the predictions of our CFD steady simulation, aiming at obtaining a reliable CFD simulation to predict the behavior of a wing in ground effect. Specifically, the values of the lift and drag coefficients are compared quantitatively by calculating the relative error from the tabulated values. As for the values of pressure coefficients, they are only qualitatively compared by means of a plot.

## II. MODELS AND METHODS

### A. Problem geometry

The geometry taken into account is the "main" element described in [2]<sup>1</sup>. It consists of one General Aviation-Whitcomb (GAW) airfoil suitably modified in order to reduce the wake behind the airfoil itself. Such geometry is shown in fig. 1.

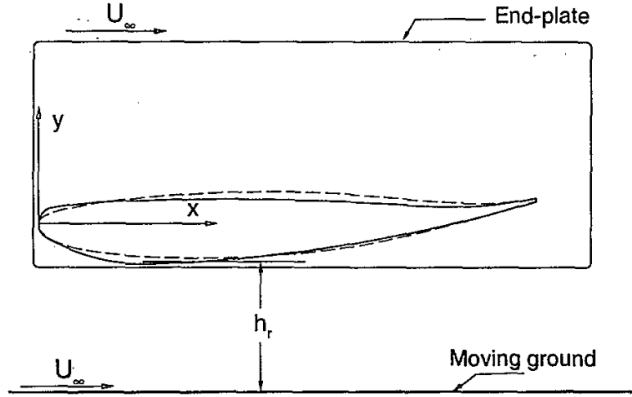


Fig. 1: A side view of wing model with end-plates at ride height  $h_r$ . The image is taken from [1].

In the actual experiment, endplates were used to control 3D effects around the airfoil; this allows our 2D simulation to be closer to that configuration. Several experiments based on the distance from the ground have been carried out: the height varies between 11.17 mm and 225.6 mm. The geometrical quantities that characterize the airfoil are the chord  $c = 223.4$  mm, and a resulting incidence, for the endplates parallel to the ground equal to  $1^\circ$ . In the reference paper, the experiment was carried out in two different wind tunnels, and since the majority of results were obtained in the  $2.1 \times 1.7$  m wind tunnel, the domain considered has the same dimensions. The height of the airfoil above the ground was parameterized and the CFD simulation was run for 17 different values of  $h/c$ .

### B. Physical modeling and hypotheses

The fluid considered in the simulation is air at standard conditions (Newtonian fluid) and has been considered incompressible since values of flow velocity are such that the Mach number is  $M \ll 0.3$ . The dynamic viscosity is  $\mu = 1.7894 \times 10^{-5}$  kg/ms and the density is  $\rho = 1.225$  kg/m<sup>3</sup>. The upstream velocity is  $U_\infty = 30$  m/s, yielding a dynamic pressure  $q_\infty = 551.625$  Pa<sup>2</sup>. Turbulence was modeled using Spalart-Allmaras one-equation model: such a model is particularly suitable for aerodynamic problems. As the Ansys Fluent guide states [6], the 2021 version of the Spalart-Allmaras

<sup>1</sup>In this Ph.D. dissertation, the geometry investigated was made out of two elements, the wing (main element) and a flap.

<sup>2</sup> $q_\infty = 56.25$  mm water.

model can deal with any value of  $y^+$ . That said, in the original formulation it is “a low-Reynolds number model, requiring the viscosity-affected region of the boundary layer to be properly resolved”, therefore we opted for a value of  $y^+$  associated with the first cell on the airfoil  $y^+ \approx 1$ . The mesh was thus appropriately created to match  $y^+ \approx 1$  (see Section II-D for further details).

### C. Boundary conditions

In the wind tunnel, the authors made use of a moving belt to simulate realistic conditions of a vehicle moving through still air: this condition was imposed in Fluent, giving to the bottom edge of the domain a condition of moving wall, with the same velocity as the upstream flow. For what concerns the other boundary conditions, the inlet condition is that of a constant velocity magnitude  $u_\infty$  parallel to the  $x$ -axis, with a known turbulence intensity (as declared in [3]), and a reasonable value for a wind tunnel of the integral turbulent scale  $l_i = 1$  cm. The boundary condition imposed on the upper edge of the domain is that of a stationary wall (no-slip condition), while the condition at the outlet is that of a pressure outlet, with default value  $p = 0$  Pa.

### D. Computational mesh

The following are the characteristics of the final mesh obtained after the mesh convergence study (see Section II-F). An unstructured mesh was created using triangular elements and two bodies of influence, starting from the geometry shown in fig. 2, with an element size of  $5.5 \times 10^{-3}$  m.

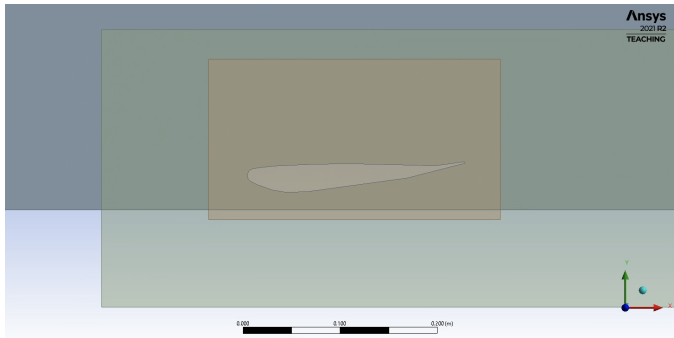


Fig. 2: Geometry of the problem. Both bodies of influence are visible (light green and light brown).

Two rectangular bodies of influence were created. The horizontal body of influence (light green in fig. 2) is used to decrease the size of the elements in the region most affected by the presence of the airfoil and in its wake. Here the element size is imposed equal to  $3 \times 10^{-3}$  m. The “vertical” body of influence (light brown in fig. 2) is used to further decrease such size over and under the airfoil itself. Here the element size is decreased to  $1.05 \times 10^{-3}$  m. This is because the greatest gradients of velocity and pressure are located in the region between the airfoil and the ground, and in the wake of the airfoil. Inflations were used both over the airfoil and on the moving belt. Over the airfoil surface, a first layer thickness of

$1 \times 10^{-5}$  m was used in order to obtain a value of normalized height  $y^+ \approx 1$ . Such thickness was computed beforehand according to [5]. After running the simulation, the trend of  $y^+$  was plotted to check the correctness of the value of  $y^+$ . An edge sizing with element size equal to  $6.5 \times 10^{-4}$  m was used over the entire airfoil contour. The trailing edge is not sharp, but has a finite thickness: it was therefore partitioned into up to 7 elements. The growth of the elements in the inflation was controlled to get an area of the last element of the inflation comparable with the area of the first element of the outside domain. For what concerns the quality of the mesh, values of skewness  $< 0.7$  and orthogonality  $> 0.2$  were considered indicators of a good meshing process. The resulting mesh is shown in fig. 3, while details of the leading and trailing edge of the resulting mesh are shown in fig. 4 and 5, respectively.

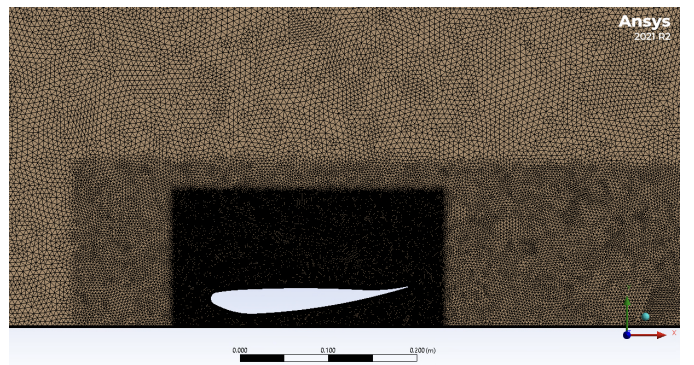


Fig. 3: Resulting mesh.

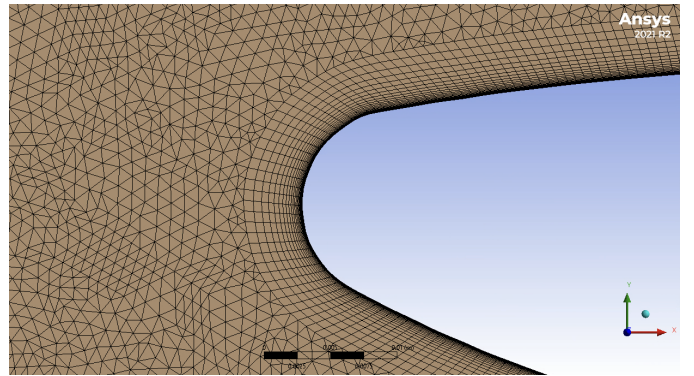


Fig. 4: Resulting mesh (detail of the leading edge).

### E. Numerical methods

In Fluent, a finite volume method is adopted. The simulation run is steady, and a pressure-based solver was employed. A coupled solver was used, with a second-order approximation of both momentum and mass equation. The convergence criteria were given by either the reach of a given tolerance on the residuals  $1 \times 10^{-4}$  or a number of iterations exceeding 500. A hybrid initialization was used.

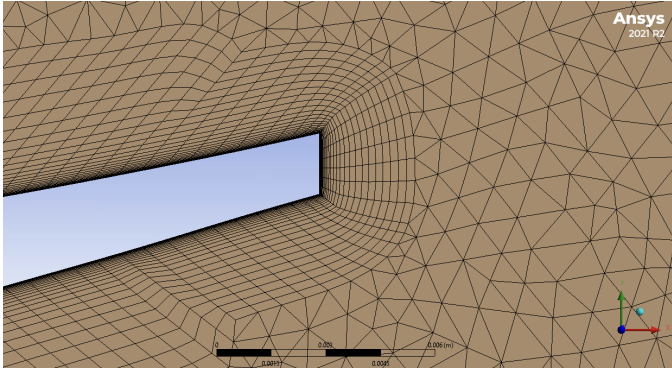


Fig. 5: Resulting mesh (detail of the trailing edge).

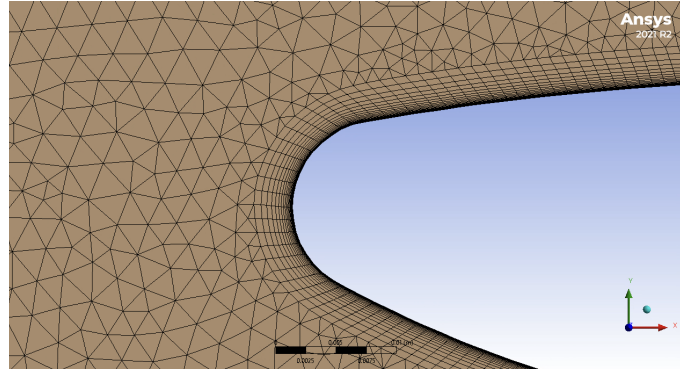


Fig. 8: Coarsest mesh (detail of the leading edge).

#### F. Mesh convergence study

The mesh convergence was assessed by reducing the size of the elements in the bodies of influence and correcting the inflation parameters to keep the mesh quality indicators in the above-defined ranges. Fig. 6, fig. 7 and fig. 8 show the coarsest mesh considered (first point in the plot in fig. 9).



Fig. 6: Coarsest mesh.

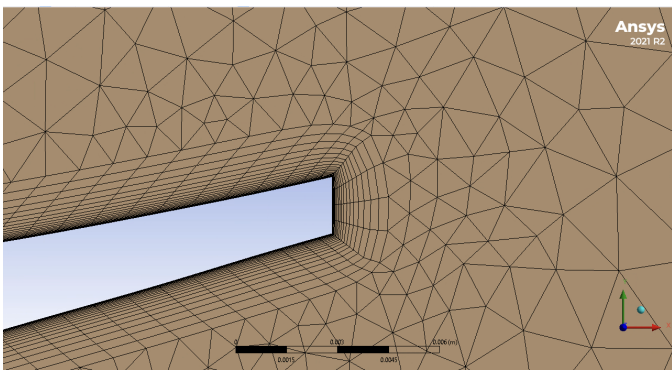


Fig. 7: Coarsest mesh (detail of the trailing edge).

Then, the simulation was carried out by computing, for each new mesh, the value of  $c_L$  and  $c_D$  for a fixed value of  $h/c = 0.11$ . In the end, only  $c_L$  was used to assess mesh convergence. This was done not only because usually  $c_L$  constitutes the most relevant aerodynamic quantity for a wing in ground effect but also because the relative error estimate for  $c_D$  is significantly

small regardless of the fineness of the mesh (see Appendix A for details). The results are shown in fig. 9, where both the trend of  $c_L$  and its relative error are plotted. Note that the relative error is below 1% already for a number of elements around 300000.

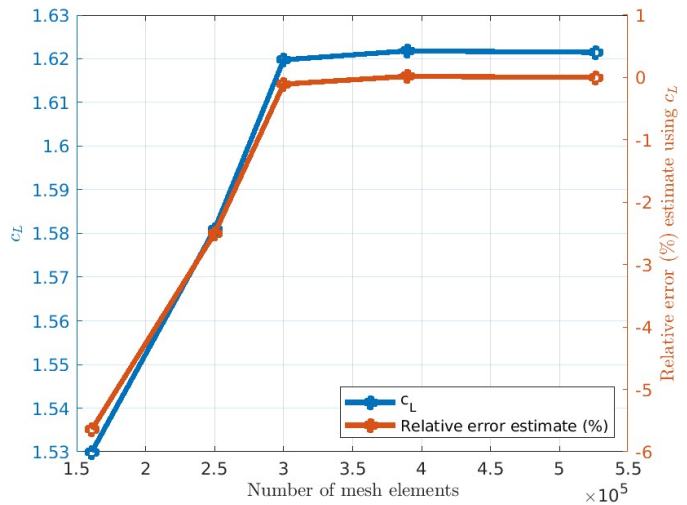


Fig. 9: Mesh convergence study.  $c_L$  is computed at  $h/c = 0.11$ , and the relative error is computed with respect to the value for the finest mesh.

To ensure convergence, for all the further computations a mesh with the characteristics of the one with roughly 380000 elements was used<sup>3</sup> since the value of  $c_L$  does not change significantly for finer meshes.

#### G. Validation quantities

Once obtained from the paper, both  $c_L(h/c)$  and  $c_D(h/c)$  were computed through the CFD simulation, along with the pressure coefficient  $c_p$  for two different ride heights:  $h/c = 0.07$  and  $h/c = 1.01$ . The first height corresponds to the case for which the highest  $c_L$  was obtained experimentally; the second one was chosen because it represents the case of negligible ground effect. The results were plotted against the

<sup>3</sup>The number of elements changes with  $h/c$  since the dimensions of the bodies of influence change accordingly.

actual values, and the accordance of the CFD with the real values was assessed.

#### H. About obtaining data from the paper

In order to compare the results obtained through the CFD simulation and the experimental results, values of  $c_L$ ,  $c_D$  and  $c_p$  were extracted from the article [1]. The Matlab script `image_digitalizer.m` was used for this scope, available here. The collecting-data procedure inevitably constitutes a source of error, since the points are arbitrarily extracted and are affected by an absolute error equal to about half the thickness of the curve considered. Note that no countermeasure has been adopted in order to improve this problem. In any case, it is deemed appropriate to point out this likely source of error.

#### I. About comparing simulated and experimental results

The values of the parameter  $h/c$  used in the simulation do not match the values of  $h/c$  for which  $c_L$  was computed experimentally (i.e. all the points presented in the paper) but are distributed so as to capture correctly the trend of  $c_L$ , and the same happens for  $c_D$ . For the computation of the relative error between the simulated and experimental values, the experimental quantities were linearly interpolated in order to have at disposal the experimental values at the simulated  $h/c$ . Finally, note that an additional value of  $c_D$  and  $c_L$  for  $h/c = 0.7$  was extrapolated to be able to compare the simulated values.

### III. RESULTS

Fig. 10 shows  $c_L$  against  $h/c$  as obtained through the simulation and experimentally. The relative error of  $c_L$  is displayed in fig. 11. The trend of  $c_D$  and its relative error is shown in fig. 12 and 13.

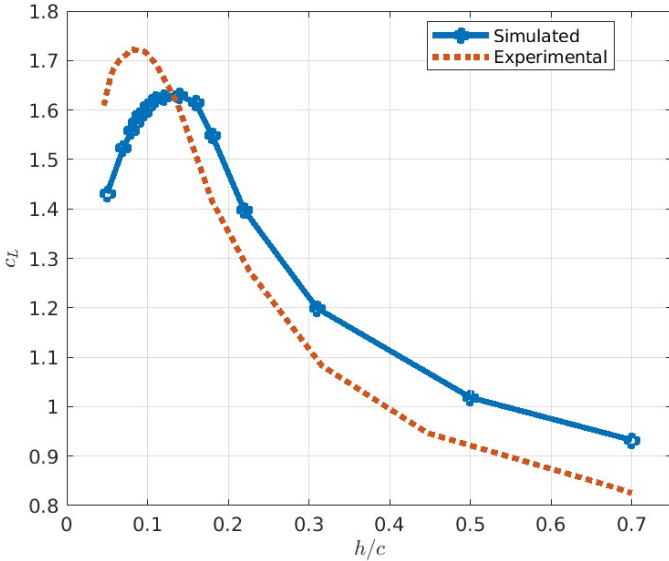


Fig. 10: Computed and experimental  $c_L$  against  $h/c$ .

Fig. 14 shows how the pressure coefficient behaves for  $h/c = 0.07$ , compared to the respective experimental trend. Fig. 15 shows the same for  $h/c = 1.01$ .

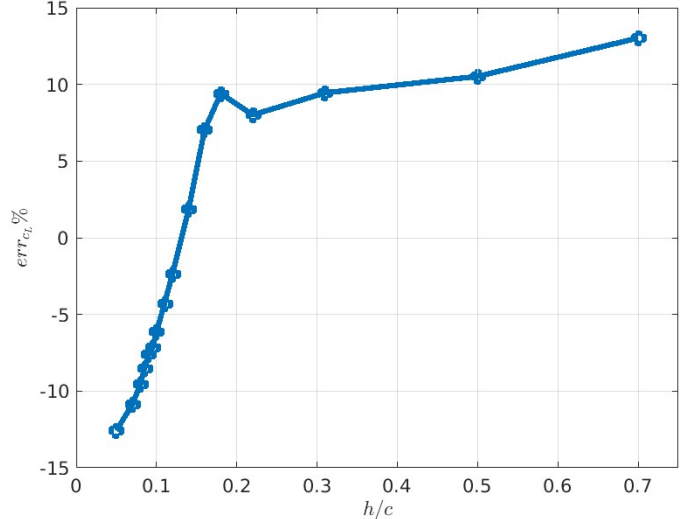


Fig. 11:  $c_L$  relative error.

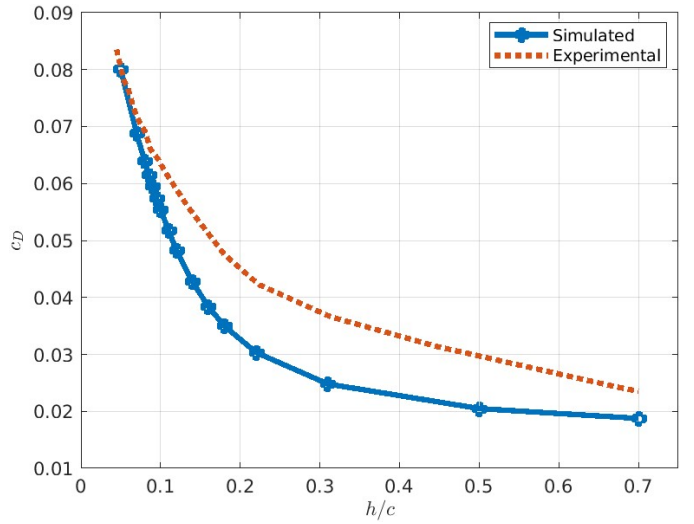


Fig. 12: Computed and experimental  $c_D$  against  $h/c$ .

Finally, fig. 16, fig. 17 and fig. 18 show the contour of velocity and the streamlines, for  $h/c = 1.01$ ,  $h/c = 0.11$  and  $h/c = 0.07$ , respectively.

### IV. DISCUSSION

The CFD simulation manages to capture the trend of  $c_L$ , despite not matching its maximum value. Additionally, the maximum is obtained for a value of  $h/c = 0.12$  instead of  $h/c = 0.07$ . While for small values of  $h/c$  the simulation underestimates the  $c_L$ , the opposite phenomenon takes place for higher  $h/c$ . This can be explained by the fact that in the free stream case (i.e.  $h/c$  sufficiently large), the 2D simulation tends to produce higher values of  $c_L$  since the aspect ratio  $AR$  of an infinite wing tends to infinity, while the 3D wing has an  $AR = 4.92$ : phenomena such as the formation of tip vortices are not predicted by the 2D simulation and, despite the presence of the endplates, the finite wing produces less downforce than the 2D airfoil. Conversely, for  $h/c < 0.15$

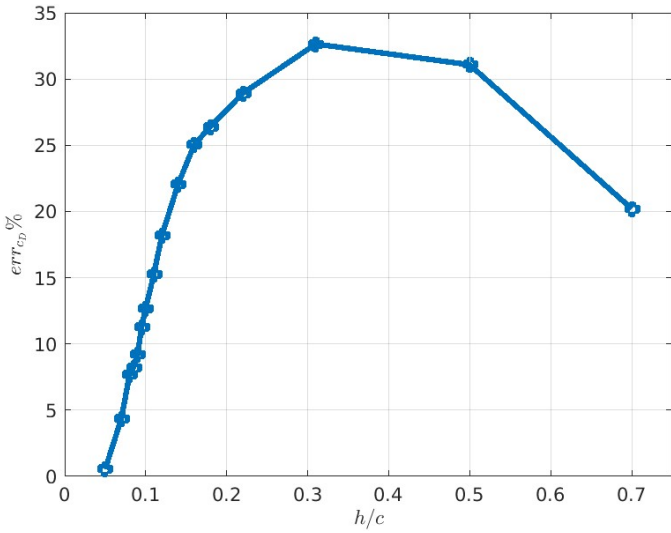


Fig. 13:  $c_D$  relative error.

the ground effect increases the  $c_L$  more than the simulation is able to show. Not only may the mesh topology need to be improved, especially near the leading edge, but we hypothesize that the turbulence in the wind tunnel as presented in [3] may not be the same condition of the experiment presented in [1]. This would explain why for small values of  $h/c$ , as shown in fig. 14 for  $h/c = 0.07$ , the  $c_p$  on the lower surface of the airfoil reaches an experimental minimum smaller than the simulated one and separation occurs later on along the chord in the wind tunnel case<sup>4</sup>. Greater turbulence and a consequently more energetic boundary layer may be the explanation for such discrepancy.

The simulated  $c_D$  matches the experimental one as long as  $h/c < 0.1$ ; after this value, the simulation computes

<sup>4</sup>Separation is visible in the  $c_p$  plot when the gradient of the suction side of the airfoil becomes small and approximately null.

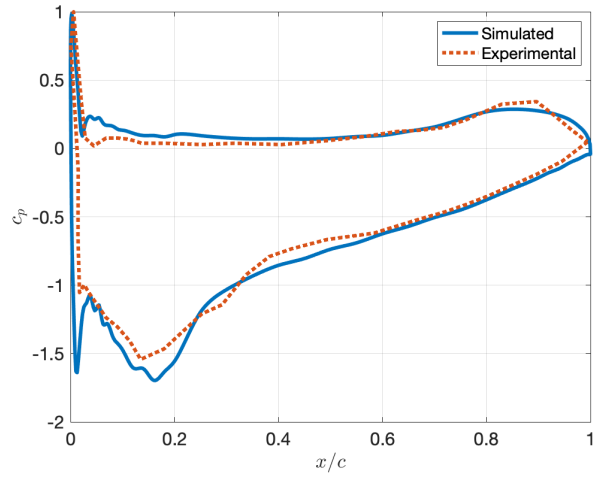


Fig. 15:  $c_p$  for  $h/c = 1.01$ .

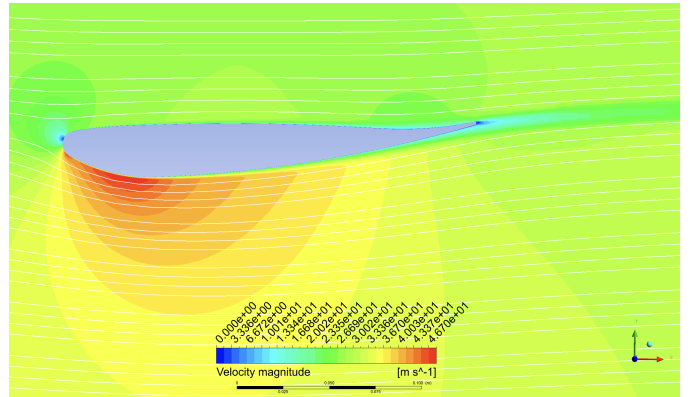


Fig. 16: Velocity contour and streamlines for  $h/c = 1.01$ . In this case no separation region is visible.

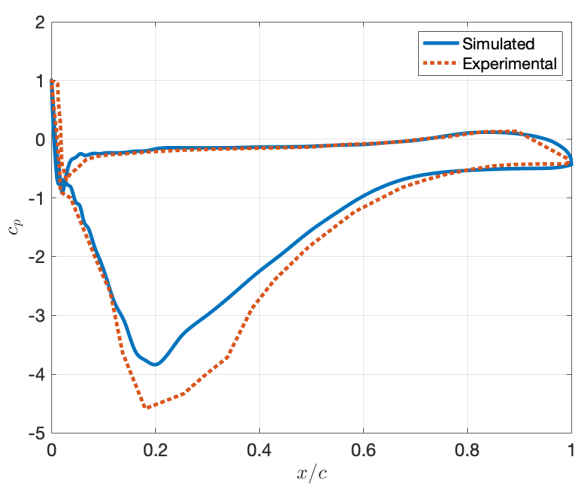


Fig. 14:  $c_p$  for  $h/c = 0.07$ .

a drag smaller than the real one. Once again this kind of phenomenon is tightly linked to the nature of the simulation: the 2D simulation does not account for the finiteness of the wing and the induced drag produced by it.

The relative error trend for  $c_L$  is a consequence of the different  $h/c$  for which the maximum is reached: the relative error  $err$  is equal to  $\approx -13\%$  for small values of  $h/c$ , then goes to 0 when the experimental and simulated curves intersect, and subsequently increases again around  $13\%$ . Such values are overall restrained and thus may confirm the reliability of the simulation. Fig. 11 shows that for  $h/c$  sufficiently large the relative error seems to become almost constant. This suggests that it is reached, for the free stream case, a contribution to the error that is no longer due to the distance from the ground, i.e. it is no longer due to the incapability of the simulation to wholly capture the ground effect phenomenon. That said, the simulation could be run for higher values of  $h/c$  to prove the correctness of such a hypothesis. For what concerns  $c_p$ , fig. 14 and fig. 15 show that the 2D simulation is able to predict the overall trend of the pressure distribution on the airfoil's surface. That said, it is also noticeable that for  $h/c = 0.07$  the

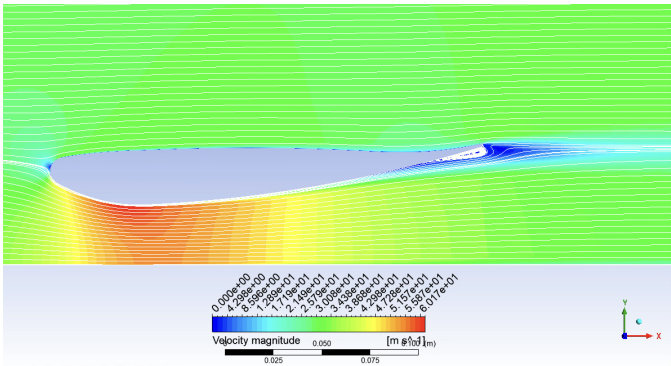


Fig. 17: Velocity contour and streamlines for  $h/c = 0.11$ . Note how the separation affects only a small portion of the airfoil suction side.

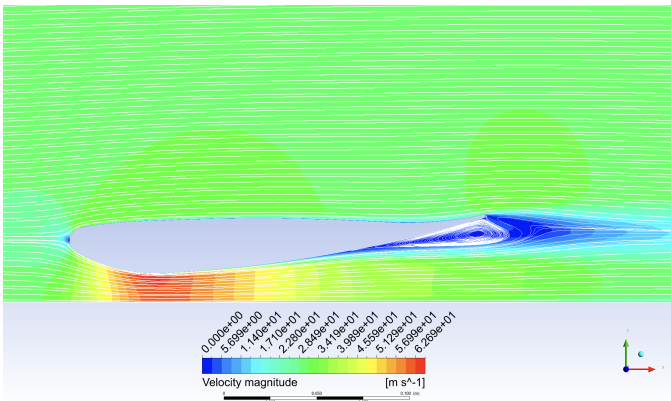


Fig. 18: Velocity contour and streamlines for  $h/c = 0.07$ . Note the region of circulation that is generated after separation.

suction peak obtained through the simulation is appreciably lower than the one presented in the experimental data. This could be due to the aforementioned turbulence intensity value used in the simulation, which may not be the actual value used in the experiment presented in the article. As already stated, this might also explain why the separation occurs further downstream in the wind tunnel experiment considered in the paper. Additionally, in both  $c_p$  plots oscillations can be seen in the vicinity of the leading edge. This highlights the limits of the adopted mesh topology. Finally, it can also be noted that the pressure coefficient data extracted from the paper, especially near the leading edge, are significantly affected by uncertainty: the plot from which these values are extracted is in fact extremely chaotic near the leading edge. A better comparison could be carried out if the actual raw data were at our disposal. Finally, fig. 17 and 18 highlight, for  $h/c = 0.11$  and  $h/c = 0.07$ , the presence of an increasing region of separation that constitutes the reason why the airfoil stalls when close to the ground. In particular, for  $h/c = 0.07$ , approximately one-third of the chord length is subjected to separation, and therefore the downforce produced is smaller than the case with  $h/c = 0.11$ . On the contrary, for the free stream case  $h/c = 1.01$ , fig. 16 shows no circulation region and the downforce is almost entirely due to the curvature of

the airfoil rather than the acceleration of the flow under it, as a consequence of the Venturi effect.

## V. SUMMARY

The 2D simulation considered succeeds in capturing almost all aspects of wind tunnel simulation: downforce, drag, and pressure coefficients obtained through the simulation are sufficiently close to those presented in [1]. Future work could aim to correct the slight inconsistencies in the results obtained for lift and drag coefficient, perhaps even with a 3D simulation. More sophisticated mesh topologies could be investigated in order to better control the pressure coefficient fluctuations near the leading edge, with higher computational power (e.g. a mesh similar to fig. 1 shown in [4]). A study regarding the wake produced by the profile could be carried out, in order to verify and compare that result as well. On the whole, the implemented simulation can be used as a first rule-of-thumb to study the behavior of a wing in ground effect.

## REFERENCES

- [1] J. Zerihan and X. Zhang, “Aerodynamics of a single element wing in ground effect,” *Journal of Aircraft - J AIRCRAFT*, vol. 37, pp. 1058–1064, Jan. 2000. DOI: 10.2514/2.2711.
- [2] J. Zerihan, “An investigation into the aerodynamics of wings in ground effect,” Ph.D. dissertation, University of Southampton, Apr. 2001. [Online]. Available: <https://eprints.soton.ac.uk/426058/>.
- [3] X. Zhang and J. Zerihan, “Aerodynamics of a double-element wing in ground effect,” *AIAA Journal*, vol. 41, no. 6, pp. 1007–1016, 2003. DOI: 10.2514/2.2057. eprint: <https://doi.org/10.2514/2.2057>. [Online]. Available: <https://doi.org/10.2514/2.2057>.
- [4] S. Wordley and J. Saunders, “Aerodynamics for formula sae: A numerical, wind tunnel and on-track study,” Apr. 2006. DOI: 10.4271/2006-01-0808.
- [5] *Y plus wall distance estimation*, Jun. 2011. [Online]. Available: [https://www.cfd-online.com/Wiki/Y\\_plus\\_wall\\_distance\\_estimation](https://www.cfd-online.com/Wiki/Y_plus_wall_distance_estimation).
- [6] *Ansys fluent theory guide*, Ansys Inc., Jul. 2021, p. 45.

## APPENDIX A

### MESH CONVERGENCE STUDY: TREND OF $c_D$

Fig. 19 shows how the value of  $c_D$  changes when refining the computational mesh, and the relative value computed with respect to the finest mesh value. Note that the relative error is, in absolute value, always smaller than 0.25%. This justifies the use of  $c_L$  rather than  $c_D$  to assess the mesh convergence.

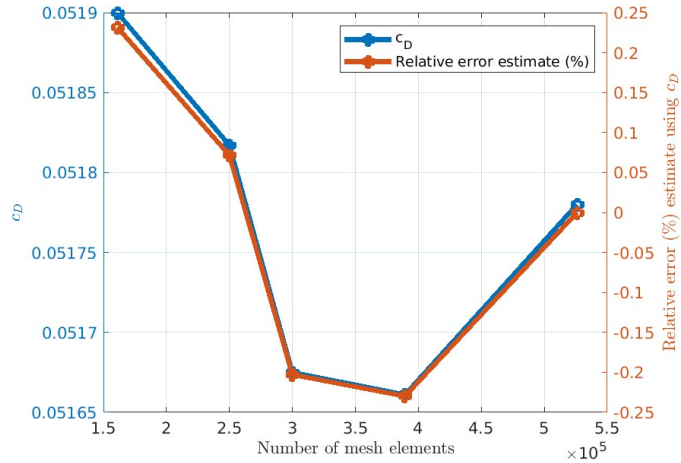


Fig. 19: Mesh convergence study.  $c_D$  is computed at  $h/c = 0.11$ , and the relative error is computed with respect to the value for the finest mesh.